Egypt. J. Chem. **Vol. 66**, No. 3. pp. 209 - 231 (2023)

Egyptian Journal of Chemistry

http://ejchem.journals.ekb.eg/

Chemical Reaction and Thermal Radiation via Cattaneo-Christov Double Diffusion (CCDD) Effects on Squeezing Non-Netonian Nanofluid Flow between Two – Parallel Plates

Yasmeen M. Mohamed, Nabil T. M. El-Dabe, Mohamed Y. Abou-zeid, Mahmoud E. Oauf and Doaa R. Mostapha

Department of Mathematics, Faculty of Education, Ain Shams University, Roxy, Cairo, Egypt

Abstract

The influences of Cattaneo-Christov double diffusion (CCDD) of an incompressible nanofluid flow is examined. The fluid is obeying Eyring – Powell model. The fluid flows amidst two - parallel plates which are vertical. The impacts of Soret number, porous medium, heat generation and thermal radiation are taken into consideration. A suitable similarity transformation is utilized to convert the controlling system of non-linear partial differential equations to ordinary ones. Moreover, the semi-analytical solutions of these equations are taken out by the means of homotopy perturbation procedure (HPM) up to second order. The influences of the distinct several physical embedded parameters on the allocations of velocity, stream function, temperature and nanofluid concentration are pointed out via a collection of graphs. Furthermore, the values of physical quantities of our interest "skin friction coefficient and nano Sherwood number" are computed and presented graphically through some draws. It's detected that the velocity has a dual performance under the impacts of the different physical parameters. Hence, it enhances with a development in the value of Darcy parameter along the interval $\eta \in [0, 0.5]$. However, at remaining interval, the vice versa occurred. On the contrast, the magnetic field parameter has an inverse conduct on the velocity when compared with the Darcy number. In addition, the velocity enriches with an increment in the value of the squeezing parameter. On the other hand, the value of the temperature declines with the enhancement in the value of thermal relaxation time. Moreover, the elevate in thermophoresis parameter leads to an enlargement in the value of nanofluid concentration. At the end, the nano Sherwood number has a dual behaviour under the impact of the Brownian motion parameter. From the physical illustration, current investigation of squeezing flow has great relevance in view of various applications. Such as injection shaping, squeezing film pressure sensors, flow rheostats, bearings, polymer industries, liquid-metal lubrication, compression and injection shaping, and food processing, etc.

Keywords: Squeezing flow; Eyring - Powell model; Nanofluid; Cattaneo-Christov double diffusion (CCDD); Chemical reaction, Heat generation, Thermal radiation.

1. Introduction

Presently, nanofluids are extremely important in various engineering applications. These kind of fluids are utilized in several chemical and biomedical engineering processes. The major stimulus of appointing these fluids is to adjust the heat transfer and thermal conductivity to reach the better goaling. For example, nanofluids are utilized to enhance the rate of heat transfer of microchips in computers, transportation, defense and ships, space technology, fuel cells, food processing, nuclear reactor coolant, solid-state lightening, microelectronics, boiler flue gas temperature reduction, biomedicine, and manufacturing [1]. Dogonchi and Ganji [2] worked on the unsteady squeezing MHD nanofluid flow and heat transfer between two parallel plates in the presence of thermal radiation effect. Cattaneo–Christov heat flux model is taken into their consideration. In their analysis, they observed that the temperature distribution is lesser in the case of Cattaneo–Christov heat flux model when compared with Fourier's law. Moreover, Nusselt number is an increasing function of heat source parameter. Shehzad et al. [3] deliberated the viscoelastic micropolar fluid in the presence of nanoparticles. Also, the thermal radiation impacts are contributed to the temperature equation. The semi-analytical

* Corresponding author email: yasmeenmostafa3038@yahoo.com
Receive Date: 17 June 2022, Revise Date: 30 June 2022, Accept Date: 04 July 2022
DOI:10.21608/EJCHEM.2022.145286.6332

solutions to these expressions have been tackled by the homotopy analysis method.

The study of non-Newtonian materials is highly significant in engineering and the applied science fields. There are various rheological models which utilizing to analyze and display the features of flow and transfer of heat. Among these non-Newtonian models there is Eyring - Powell liquid model. This model is very complicated mathematically However, it gains great interest because of the following reasons. Firstly, its constitutive relationship is given empirically. Secondly Newtonian behavior appears for both low and high shear stresses. This model in presence of heat transfer plays an essential role in different industrial, natural, and geophysical processes which include delivery of dampness and temperature over environmental pollution, damaging of crops due to freezing, underground energy transport, geothermal reservoirs, thermal insulation, and agricultural fields. In addition, the Eyring-Powell fluid has got substantial attentions due to the following rationales, "Instead of empirical relation it is derived by using kinetic theory of liquid" and "It behaves like Newtonian fluid under low and high shear rates" [4]. Thus, recently there are scholars who are working on Eyring-Powell fluid model. For example, Ibrahim [5] examined three-dimensional boundary layer flow of a rotating Powell-Eyring nanofluid. In their study heat transfer processes, non-Fourier heat flux theory and for mass transfer non-Fick's mass flux theory are considered. In their investigation, they realized that the non-Newtonian fluid parameter N has the characteristic of reducing the amount of local Nusselt numbers. Ibrahim and Hindebu [6] elaborated the MHD boundary layer flow of Eyring-Powell nanofluid over stretching cylinder with Cattaneo-Christov heat flux model. Through their investigation, they found that the velocity profile enhances with an enlargement in the value of the Eyring-Powell fluid parameter. However, it decays as the magnetic parameter enlarges. Both the temperature and the concentration profiles have revealed an enhancement pattern for high values of the magnetic parameter.

Lately, researchers and scientists dedicated their interest to analyse the demeanour of viscous fluid flows disfigured by squeezing surfaces because of their several useful applications related to engineering, the industrial process, and biomedical such as polymer process, in designing of motor bearings and electro-rheological fluids utilized to manufacture dampers, bubble boundaries shrink in depth and expand bi-axially, liquid-metal lubrication, foams. There are some other examples of squeezing flow corresponding to bioengineering and mathematical biology involving diarthrodial joints [7]. The work on squeezing flow is first introduced by Stefan [8]. Atlas et al. [9] Scrutinized the influence of entropy generation on two-dimensional unsteady Casson fluid flow squeezing between two parallel plates. It is noticed that the entropy generation profile enhances with an increase in the values of the Brinkman and Reynolds numbers. the heat and mass transfer in an unsteady two-dimensional squeezing flow of magnetohydromagnetic (MHD) radiative non-Newtonian Eyring-Powell fluid between two parallel infinite plates is deliberated by Ghadikolaei et al. [10]. It's found that the value of the velocity decreases with an enhancement in the value of magnetic field parameter. Also, their temperature value reduces by increasing in the value of thermal radiation parameter. Hosseinzadeh et al. [11] explored the heat and mass transfer of MHD nanofluid squeezing flow between two parallel plates. In their work, it's recognized that the increase in the value of Brownian motion parameter leads to an increase in the value of the temperature. The Transient electromagnetohydrodynamic radiative squeezing flow between two parallel Riga plates using a spectral local linearization approach is reported by Thumma and Magagula [12]. Rasool et al. [13] elaborates the magnetohydrodynamics and Darcy - Forchheimer medium in nanofluid flow between two horizontal plates.

Heat and mass transport combined phenomenon plays a substantial role significantly in several industrial and engineering processes, as, equipment power collectors, damage of crops, food processing, refrigeration, heat exchangers, and so on. In literature, convectional transport theories for heat and mass are utilized by several researchers. But infinite speed of wave propagation led these convectional theories to be insufficient [14]. Heat and mass transfer phenomenon is described by several preceding investigations. Thus, El dabe et al. [15] examined the peristaltic flow of Jeffry nanofluid with heat transfer through a porous medium in a vertical tube. El-dabe and Sallam [16] investigated the impact of non-Darcy Couette flow through a porous medium of magnetohydrodynamic viscoelastic fluid with heat and mass transfer. El dabe et al. [17] analysed the effect of heat transfer on MHD non-Newtonian Casson fluid flow between two rotating cylinders. El-dabe and Mohamed [18] studied the influence of heat and mass transfer in hydromagnetic flow of the non-Newtonian fluid with heat source over an accelerating surface through a porous medium. El dabe et al. [19] explained the impact of wall properties on the peristaltic motion of a coupled stress fluid with heat and mass transfer through a porous medium. El-dabe and Abou-zeid [20] discussed the influence of radially varying magnetic field on peristaltic motion with heat and mass transfer

of a non-Newtonian fluid between two co-axial tubes. Fourier [21] is the first one who present the law of heat conduction and the properties of heat transfer. Thus, in this regard, traditional Fourier's law is modified to involve thermal relaxation time by Cattaneo [22], which means that heat is transported in normal way. Fourier's heat expression is a parabolic energy equation, meanwhile, Cattaneo's equation leads to hyperbolic type energy equation. Christov [23] modified the work of Cattaneo. Similarly, Fick's law plays a significant role for studying mass transport. Cattaneo - Christov model is examined by several related numerical previous investigations can be found in Refs. [24-28].

Various numerical techniques were utilized to examine enormous domain of linear as well as nonlinear phenomena in physical, engineering, and mathematical problems. On the other hand, many efforts had been performed to tackle these phenomena, analytically, starting from the traditional perturbation methods till to the multiple time scale method. The straightforwardness of the perturbation methods, in it transforms the nonlinear equations into linear ones. Indeed, all these perturbation methods depend mainly on a small built-in parameter. Thereafter, the existence of such a parameter is fundamental to gain an approximate solution of the given problem. Usually, the solution of a problem may be restricted by the continuation of this parameter. The homotopy perturbation method (HPM) is one of the momentous techniques, first proposed by He [29] in 1999 is considered as the first one, who overcomes this difficulty, by representing the HPM. The principal advantage of this method comes from it does not depend on a built-in small parameter in the system of equations. Moreover, the approximated solutions are uniformly valid, not only for small parameter, but also at large one. Throughout, this hopeful method, an artificial parameter $P \in [0,1]$ is incorporated into the problem, to divide it into; two linear and nonlinear parts. It is sometimes known as the homotopy parameter. This method had been successfully utilized for solving linear and nonlinear partial as well as ordinary differential equations. Throughout this work, He produced a modified one of the standard homotopy and the perturbation techniques by improving the HPM for solving linear, nonlinear, initial, and boundary value problems. This method has a significant characteristic in that it delivers an analytical approximate solution to the extensive variety of linear and nonlinear problems in the applied sciences. He's homotopy perturbation method is elucidated as an appropriate with the multipurpose nature of the various physical problems. It has been in a great large class of functional equations and the references therein. Setting $P = 0$, implies that the differential equation takes a simplified form. As P is enriched and reaches unity $(P = 1)$, in the end, the equation improves to the desired form. At this step, the anticipated solution will be approached to the required formula.

The governing equations relevant to our resultant one become more complicate to treat as supplemental nonlinear terms appear in the equations of motion because of the flow performance of non-Newtonian nanofluids flow with Cattaneo-Christov heat and mass fluxes. Thus, the exact solutions of such problems are virtually impossible. Thus, some researchers obtained numerical solutions for these problems [30 - 39]. We turn to find a semi analytical solution by means of homotopy perturbation method (HPM). On design the homotopy perturbation technique, the given differential equations and their relevant boundary conditions are converted into another simple system of these equations which leads to a power series solution of these equations.

Based on the above literature survey, Most of the existing analytical studies didn't discuss nanofluid flow via Cattaneo–Christov double diffusive model corrected mathematically. Since some extra terms relevant to Brownian motion and thermophoresis effects appear under the theory of Cattaneo–Christov, that are missing in these previous published studies. Here, our essential Theme is to cover such analysis in order to optimize the mathematical data with real situations. The influence of squeezing Eyring - Powell nanofluid via Cattaneo-Christov double diffusion (CCDD) model between two parallel vertical plates in the presence of time is analyzed. Thermal radiation, porous medium, uniform magnetic field in addition heat generation are taken into consideration. Variable surface temperature and convected boundary condition are also considered. A proper similarity transformations is applied to convert our system from partial differential equations to ordinary differential equations for solving it easily. Homotopy perturbation method (HPM) up to second order is applied to obtain the semi-analytical solution for the velocity, stream function, temperature, and nanoparticle concentration distributions. The values of skin friction, and nano Sherwood number are also calculated and exhibits via a set of diagrams.

Physiologically, according to the geometry of squeezing is realized that squeezing the fluids have a great interest in view of diverse various applications. Like food, polymer industries, compression and injection shaping and liquid-metal lubrication, etc. In view of applications, the nanofluids applications may be introduced as: energy storage, chemical industry, power production, heat exchangers, refrigeration process, etc. The observed results due to flow over

two-parallel plates embedded in a porous medium have several applications in diverse areas of science and technological fields, namely st

udy of ground water resources in agricultural engineering, in petroleum technology to study the moment of ordinary gas, oil, and water through the oil reservoirs. MHD provides a mean of cooling the turbine blade and keeping the structural integrity of the nose cone. Moreover, the obtained results that have been obtained from our study can be used in many various applications. Like, develops and manufactures wellhead control panels, and chemical injection systems. Including wellhead safety control systems, metallurgical process, polymer

The strategy of the current work can be performed as follows: Sec. 2 clarifies the mathematical explanation of the problem. A description of the problem comprising the governing equations of motion of the considered system as well as the appropriate boundary conditions are illustrated throughout Sec. 3. Sec. 4 visualizes the method of solutions of the system of equations. The numerical results and discussion of the various physical parameters are examined in Sec. 5. Finally, concluding remarks of the current study are represented throughout Sec. 6.

2. Mathematical description

2.1 Theory and analysis of the fluid flow

The flow is deemed to be an unsteady and incompressible two-dimensional flow of Eying - Powell nanofluid. The fluid flows between two vertical parallel plates separated through a time dependent distance $h(t)$. The Cartesian coordinate (x, y) is applied to analyse the fluid flow. The left plate is placed at $y = 0$ and it has a variable stretching velocity $U_m(x) = ax(1-bt)^{-1}$ in x - direction. where a and $(1-bt)^{-1}$ for $\left((bt \prec 1) i.e. \left(t \prec (b)^{-1}\right)\right)$ are the initial and effective stretching rate. Meanwhile, the right plate is located at $y = h(t) = \sqrt{\upsilon_f (a)^{-1}(1-bt)}$. Squeezing flow is produced when the right plate squeezing in the direction of left wall with squeezing velocity $v_h = \frac{dh}{dt}$. The physical model is portrayed in Fig. 1

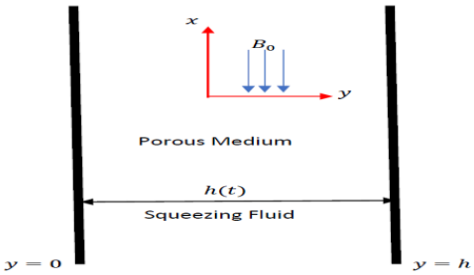

Fig(1)

The Cauchy stress tensor $\underline{S}$ for Eying - Powell model may be expressed as follows [5]:

$$\underline{S} = \left[\mu_f + \frac{1}{\beta_r \dot{\gamma}} \sinh^{-1}\left(\frac{\dot{\gamma}}{c}\right)\right] \underline{A}_1, \quad (1)$$

$$\underline{A}_1 = (\nabla \underline{V}) + (\nabla \underline{V})^T, \quad (2)$$

$$\sinh^{-1}\left(\frac{\dot{\gamma}}{c}\right) = \frac{\dot{\gamma}}{c} - \frac{1}{6}\left(\frac{\dot{\gamma}}{c}\right)^3 + \cdots, \left|\frac{\dot{\gamma}}{c}\right|^3 <<< 1. \quad (3)$$

The fluid is electrically conductive, and a uniform magnetic field is imposed orthogonally to the plates. The conductivity is usually small and therefore the magnetic Reynold's number of the flow is taken to be small enough, so that the induced magnetic field is disregarded. Also, the external electric field, and the electric field due to the polarization of charges can be ignored [40].

Considering there's no polarization voltage which the total electric field is disappearing $(\underline{E} = 0)$. Therefore, the generalized Ohm's law may be defined as [36],

$$\underline{J} = \sigma(\underline{V} \wedge \underline{B}), \quad (4)$$

According to utilizing Roseland's approximation one can take the radiative heat flux $\underline{q_r}$ in one dimension over y - axis direction. Thus, the radiative heat flux $\underline{q_r}$ can be defined as [[9], and [36]]:

$$\underline{q_r} = \frac{-4\delta_e}{3\beta_e}\frac{\partial T^4}{\partial y}, \qquad (5)$$

where, Taylor series is utilized for expanding T^4 about T_h as a linear function of temperature after neglecting higher-order terms, may be written as [[9], and [40]]

$$T^4 \approx 4T_h^3 T - 3T_h^4.$$

(6)

Energy equation can be expressed as:

$$\left(\rho c\right)_f \frac{dT}{dt} = -\nabla\cdot\underline{q} + \left(\rho c\right)_p\left[D_B\left(\nabla T\cdot\nabla C\right) + \frac{D_T}{T_f}\left(\nabla T\cdot\nabla T\right)\right] - \nabla\cdot\underline{q_r}.$$

(7)

Nanoparticles concentration equation can be defined as:

$$\frac{dC}{dt} = -\nabla\cdot\underline{j}^* + \left(\frac{D_T}{T_f} + \frac{D_B K_T}{T_m}\right)\nabla^2 T - K_1\left(C - C_f\right).$$

(8)

2.2. Analysis of Heat and mass transfer by means of Cattaneo-Christov double diffusion theory:

The theory of Cattaneo-Christov double diffusion has been represented in characterizing thermal and nanofluid concentration diffusion with heat and mass fluxes relaxations, respectively. The expressions for heat flux $\underline{q}$ and mass flux $\underline{j}^*$ in terms of Cattaneo-Christov theory are introduces as follows:

Cattaneo-Christov heat flux model may be defined as follows [[26], [27] and [28]]:

$$\underline{q} + \delta_E\left[\frac{\partial \underline{q}}{\partial t} + \underline{V}\cdot\nabla\underline{q} - \underline{q}\cdot\nabla\underline{V} + \left(\nabla\cdot\underline{V}\right)\underline{q}\right] = -K\nabla T, \qquad (9)$$

Cattaneo-Christov mass flux model can be defined as follows [[7] and [9]]:

$$\underline{j}^* + \delta_N\left[\frac{\partial \underline{j}^*}{\partial t} + \underline{V}\cdot\nabla\underline{j}^* - \underline{j}^*\cdot\nabla\underline{V} + \left(\nabla\cdot\underline{V}\right)\underline{j}^*\right] = -D_B\nabla C, \qquad (10)$$

which are the generalized Fourier's and Fick's laws, respectively. When we put $\left(\delta_E = 0\right)$ and $\left(\delta_N = 0\right)$ we can return to the classical Fourier's heat flux law and Fick's mass flux law of diffusion, respectively. For incompressible fluid we have $\left(\nabla\cdot\underline{V} = 0\right)$. Thus Eqs. (9) and (10) can be rewritten as follows:

$$\underline{q} + \delta_E\left[\frac{\partial \underline{q}}{\partial t} + \underline{V}\cdot\nabla\underline{q} - \underline{q}\cdot\nabla\underline{V}\right] = -K\nabla T, \qquad (11)$$

$$\underline{j}^* + \delta_N\left[\frac{\partial \underline{j}^*}{\partial t} + \underline{V}\cdot\nabla\underline{j}^* - \underline{j}^*\cdot\nabla\underline{V}\right] = -D_B\nabla C. \qquad (12)$$

By solving Eqs. (7) and (11) for eliminating $\underline{q}$ Also $\underline{j}^*$ can be eliminated by solving Eqs. (8) and (12).

3. The governing equations of fluid motion:

3.1. Explanation of the equations govern the motion:

The governing continuity, x - component momentum, y - component momentum, temperature, nanoparticles concentration equations may be listed as follows [[5], [9], [10], [33], and [36]]:

$$\frac{\partial u}{\partial x} + \frac{\partial v}{\partial y} = 0, \qquad (13)$$

$$\rho_f\left(\frac{\partial u}{\partial t} + \mathrm{u}\,\frac{\partial u}{\partial x} + \mathrm{v}\,\frac{\partial u}{\partial y}\right) = -\frac{\partial p}{\partial x} - \left(\sigma B_0^2 + \frac{\mu_f}{K_p}\right)u + \left(\mu_f + \frac{1}{\beta_r c}\right)\left[2\frac{\partial^2 u}{\partial x^2} + \frac{\partial^2 u}{\partial y^2} + \frac{\partial^2 v}{\partial x\partial y}\right] + \rho_f g\alpha_T\left(T - T_f\right) + \rho_f g\alpha_C\left(C - C_f\right), \qquad (14)$$

$$\rho_f\left(\frac{\partial v}{\partial t} + \mathrm{u}\,\frac{\partial v}{\partial x} + \mathrm{v}\,\frac{\partial v}{\partial y}\right) = -\frac{\partial p}{\partial y} + \left(\mu_f + \frac{1}{\beta_r c}\right)\left[2\frac{\partial^2 v}{\partial y^2} + \frac{\partial^2 v}{\partial x^2} + \frac{\partial^2 u}{\partial x\partial y}\right] - \frac{\mu_f}{K_p}u, \qquad (15)$$

$$(\rho c)_f\left(\frac{\partial T}{\partial t}+\mathrm{u}\ \frac{\partial T}{\partial x}+\mathrm{v}\ \frac{\partial T}{\partial y}\right)+\delta_E\Omega_E=K\left(\frac{\partial^2 T}{\partial x^2}+\frac{\partial^2 T}{\partial y^2}\right)$$
$$(\rho c)_p\left[D_B\left(\frac{\partial T}{\partial x}\frac{\partial C}{\partial x}+\frac{\partial T}{\partial y}\frac{\partial C}{\partial y}\right)+\frac{D_T}{T_f}\left(\left(\frac{\partial T}{\partial x}\right)^2+\left(\frac{\partial T}{\partial y}\right)^2\right)\right]$$
$$+\frac{16\delta_e T_h^3}{3\beta_e}\frac{\partial^2 T}{\partial y^2}+Q_0\left(T-T_f\right),$$

(16)

$$\frac{\partial C}{\partial t}+\mathrm{u}\ \frac{\partial C}{\partial x}+\mathrm{v}\ \frac{\partial C}{\partial y}+\delta_N\Omega_N=D_B\left(\frac{\partial^2 C}{\partial x^2}+\frac{\partial^2 C}{\partial y^2}\right)$$
$$+\left(\frac{D_T}{T_f}+\frac{D_B K_T}{T_m}\right)\left[\frac{\partial^2 T}{\partial x^2}+\frac{\partial^2 T}{\partial y^2}\right]-K_1\left(C-C_f\right),$$

(17)

where,

$$\Omega_E=(\rho c)_f\left[\begin{array}{l}\frac{\partial^2 T}{\partial t^2}+\frac{\partial u}{\partial t}\frac{\partial T}{\partial x}+\frac{\partial v}{\partial t}\frac{\partial T}{\partial y}+2\left(u\frac{\partial^2 T}{\partial x\partial t}+uv\frac{\partial^2 T}{\partial x\partial y}+v\frac{\partial^2 T}{\partial y\partial t}\right)+\\ u^2\frac{\partial^2 T}{\partial x^2}+v^2\frac{\partial^2 T}{\partial y^2}+\left(u\frac{\partial u}{\partial x}+v\frac{\partial u}{\partial y}\right)\left(\frac{\partial T}{\partial x}+\frac{\partial T}{\partial y}\right)\end{array}\right]$$
$$-\frac{16\delta_e T_h^3}{3\beta_e}\left(\frac{\partial^3 T}{\partial y^2\partial t}+u\frac{\partial^3 T}{\partial y^2\partial x}+v\frac{\partial^3 T}{\partial y^3}\right)$$
$$-(\rho c)_p\left[\begin{array}{l}D_B\left(\left(\frac{\partial T}{\partial y}\left(\frac{\partial^2 C}{\partial y\partial t}+v\frac{\partial^2 C}{\partial y^2}\right)+\frac{\partial C}{\partial y}\left(\frac{\partial^2 T}{\partial y\partial t}+u\frac{\partial^2 T}{\partial x\partial y}+v\frac{\partial^2 T}{\partial y^2}\right)\right)\right)\\ +2\frac{D_T}{T_f}\left(\frac{\partial T}{\partial x}\left(\frac{\partial^2 T}{\partial x\partial t}+v\frac{\partial^2 T}{\partial x\partial y}\right)+\frac{\partial T}{\partial y}\left(\frac{\partial^2 T}{\partial y\partial t}+u\frac{\partial^2 T}{\partial x\partial y}+v\frac{\partial^2 T}{\partial y^2}\right)\right)\end{array}\right]$$
$$-Q_0\left(\frac{\partial T}{\partial t}+u\frac{\partial T}{\partial x}+v\frac{\partial T}{\partial y}\right),$$

(18)

$$\Omega_N=\frac{\partial^2 C}{\partial t^2}+\frac{\partial v}{\partial t}\frac{\partial C}{\partial y}+2v\frac{\partial^2 C}{\partial y\partial t}+v\frac{\partial v}{\partial y}\frac{\partial C}{\partial y}+v^2\frac{\partial^2 C}{\partial y^2}$$
$$+K_1\left(\frac{\partial C}{\partial t}+v\frac{\partial C}{\partial y}\right)-\left(\frac{D_T}{T_f}+\frac{D_B K_T}{T_m}\right)\left[\frac{\partial^3 T}{\partial y^2\partial t}+u\frac{\partial^3 T}{\partial x\partial y^2}+v\frac{\partial^3 T}{\partial y^3}\right].$$

(19)

The corresponding boundary conditions may be defined as [[9], and [36]]:

$$\mathrm{u}=\mathrm{U_m},\quad \mathrm{v}=0,\qquad T(x)=T_f+\left(T_h-T_f\right)x^m,$$
$$x>0 \text{ and } C=C_h, \qquad \text{at } \mathrm{y}=0 \qquad (20)$$
$$\frac{\partial T}{\partial y}=0 \qquad \text{at } \mathrm{y}=\frac{\mathrm{h}}{2}$$

(21)

$$\mathrm{u}=0,\ \mathrm{v}=\mathrm{v_h}=\frac{dh}{dt},\ -\mathrm{K}\frac{\partial \mathrm{T}}{\partial \mathrm{y}}=\mathrm{h_t}\left(T_h-T\right),\ \text{and}$$
$$-\mathrm{D_B}\frac{\partial \mathrm{C}}{\partial \mathrm{y}}=\mathrm{h_n}\left(C_h-C\right). \qquad \text{at} \qquad \mathrm{y}=\mathrm{h}$$

(22)

Local similarity variables may be defined as follows [9]:

$$\psi=x\sqrt{\frac{a\nu_f}{(1-bt)}}f(\eta),\ u=\psi_y=U_m f'(\eta),$$
$$v=-\psi_x-\sqrt{\frac{a\nu_f}{(1-bt)}}f(\eta),\theta(\eta)=\frac{T-T_f}{T_h-T_f},$$
$$\Phi(\eta)=\frac{C-C_f}{C_h-C_f},\ \eta=\frac{y}{h(t)},\ U_m=\frac{ax}{(1-bt)}.$$

(23)

It is appropriate to write the governing system of Eqs. (13) - (19) with the corresponding boundary conditions (20) - (22) in a non-dimensional form. This can be done in several different ways depending mainly on the choice of the distinct length, mass, and time. Postulate the following non-dimensional forms: The characteristic length $=x$, the characteristic mass $=\rho_f x^3$ and the characteristic time $=(1-bt)(a)^{-1}$. The other dimensionless quantities are given as follows:

$$\varepsilon=\frac{1}{\mu\beta_r c},R_e=\frac{xU_m}{\nu_f},M^2=\frac{\sigma B_0^2x^2}{\mu_f},\theta=\frac{T-T_f}{T_h-T_f},\Phi=\frac{C-C_f}{C_h-C_f},$$
$$B_{iT}=-\frac{h_t}{K}\sqrt{\frac{\nu_f(1-bt)}{a}},B_{iN}=-\frac{h_n}{D_B}\sqrt{\frac{\nu_f(1-bt)}{a}},P_r=\frac{c_f\mu}{K},$$
$$\gamma_E=\frac{\delta_E U_m}{x},\gamma_N=\frac{\delta_N U_m}{x},G_r=\frac{gx^2\alpha_T(T_h-T_f)}{\nu_f U_m},G_c=\frac{gx^2\alpha_C(C_h-C_f)}{\nu_f U_m},$$
$$N_b=\frac{\tau D_B(C_h-C_f)}{\nu_f},N_t=\frac{\tau D_T(T_h-T_f)}{\nu_f T_f},S_r=\frac{D_B K_T(T_h-T_f)}{\nu_f T_m(C_h-C_f)},$$
$$R_d=\frac{16\delta_e T_h^3}{3K\beta_e},\tau=\frac{(\rho c)_p}{(\rho c)_f},\beta_1=\frac{Q_0x^2}{\mu c_f},\nu_f=\frac{\mu_f}{\rho_f},D_a=\frac{K_p}{x^2},L_e=\frac{\nu_f}{D_B},$$
$$R_c=\frac{K_1x^2}{\nu_f},\beta=\frac{\gamma}{a}.$$

(24)

After substituting the forgoing Eqs. (23) and (24) into Eqs. (13) - (22). Then, the governing system of non-linear ordinary differential equations may be written in the following form as:

$$R_e\left((1+\varepsilon)f'''+ff'''+\beta\left(f'-\frac{1}{2}\eta f''\right)\right)$$
$$-f'f''-\left(M^2+\frac{1}{D_a}\right)f''+G_r\theta'+G_c\Phi'=0, \quad (25)$$
$$(a_1f+a_2\eta)\theta'''+a_3\theta''+a_4f\theta'+a_5\theta'\Phi'+a_6\theta'^2+$$
$$a_7\eta^2\theta''+a_8\eta\theta'+a_9\eta f'\theta'+a_{10}\eta f\theta''+a_{11}f^2\theta''+$$
$$a_{12}ff'\theta'+a_{13}\eta\theta'\Phi''+a_{14}\eta\theta''\Phi'+a_{15}f\theta'\Phi''+$$
$$a_{16}f\theta''\Phi'+a_{17}\eta\theta'\theta''+a_{18}f\theta\theta'+a_{19}\theta+a_{20}\eta\theta'$$
$$+a_{21}f\theta'+a_{22}\theta'=0, \quad (26)$$
$$b_1\Phi''+b_2\theta''+b_3\eta\Phi'+b_4\theta'+b_5\Phi+b_6\eta\theta'''+b_7f\Phi'+$$
$$b_8\eta f'\Phi'+b_9f^2\Phi''+b_{10}ff'\Phi'+b_{11}f\theta'''+b_{12}\eta^2\Phi''$$
$$+b_{13}\eta\theta''=0.$$

(27)

The transformed boundary conditions may be written as:

$$f(0)=v_0,\ f'(0)=1,\ \theta(0)=x^m,\text{ and}$$
$$\Phi(0)=1,$$

(28)

$$\theta'\left(\frac{1}{2}\right)=0,$$

(29)
$$f(1)=\frac{\beta}{2},\ f'(1)=0,$$
$$\theta'(1)+B_{iT}\ (\theta(1)-1)=0,\quad\text{and}$$
$$\Phi'(1)+B_{iN}\ (\Phi(1)-1)=0.$$

(30)

Where the coefficients a_1-a_{22} and b_1-b_{13} that recognized into Eqs. (25) - (27) are excluded here for save space. But it available under your request.

3.2. The physical quantities of our interest may be defined as follows:

The skin friction coefficient C_F may be written as [[5], [9], and [10]]:

$$C_F=\frac{\tau_w}{\rho_f U_m^2},$$

(31)

The Nusselt number Nu_x can be written as follows [[5], [9], and [10]]:

$$Nu_x=\frac{xq_w}{K(T_h-T_f)}, \quad (32)$$

The nano-Sherwood number Sh_x may be defined as follows [[5], [9], and [10]]:

$$Sh_x=\frac{xq_m}{D_B(C_h-C_f)}.$$

(33)

where, τ_w, q_w, and q_m can be defined as:

$$\tau_w=\left(\mu_f+\frac{1}{\beta_r c}\right)\left(\frac{\partial u}{\partial y}\right)\Bigg|_{y=h},$$

(34)

$$q_w=-\left[K+\frac{16\delta_e T_h^3}{3K\beta_e}\right]\left(\frac{\partial T}{\partial y}\right)\Bigg|_{y=h},$$

(35)
$$q_m=-D_B\left(\frac{\partial C}{\partial y}\right)\Bigg|_{y=h}.$$

(36)

The non - dimensional forms for the skin friction coefficient C_F, the Nusselt number Nu_x and the nano-Sherwood number Sh_x after utilizing the similarity transformation can be defined as:

$$\sqrt{R_e}C_F = (1+\varepsilon) f''(1), \tag{37}$$

$$Nu_x = -\sqrt{R_e}(1+R_d)\theta'(1), \tag{38}$$

$$Sh_x = -\sqrt{R_e}\Phi'(1). \tag{39}$$

4. Homotopy perturbation method and analysis of convergence:

4.1. The structure of the homotopy perturbation technique:

Due to the complexity in treating the resultant system of equations, we can't solve it analytically. Therefore, with the aid of HPM, we suppose that Eqs. (25) - (27) with the appropriate boundary conditions (28) - (30) have the solution as the form:

$$G = \mathrm{H}_0 + \mathrm{P}\,\mathrm{G}_1 + \mathrm{P}^2\,\mathrm{G}_2 + \cdots\cdots, \tag{40}$$

where G refers to any physical function of the following distributions: f, θ, and Φ.

The homotopy statements for the forgoing Eqs. (25) - (27) may be formulated as follows:

$$H(P,f) = L_1(f) - L_1(f_0) + PL_1(f_0) + P\left[N_f(\eta)\right] = 0, \tag{41}$$

$$H(P,\theta) = \mathrm{L}_2(\theta) - \mathrm{L}_2(\theta_0) + P\,\mathrm{L}_2(\theta_0) + P\left[\left((a_1 f + a_2\eta)^{-1}\right)\left(N_\theta(\eta)\right)\right] = 0, \tag{42}$$

$$H(P,\Phi) = \mathrm{L}_3(\Phi) - \mathrm{L}_3(\Phi_0) + P\,\mathrm{L}_3(\Phi_0) + P\begin{bmatrix} b_2\theta'' + b_3\eta\Phi' + b_4\theta' + b_5\Phi + b_6\eta\theta''' + b_7 f\Phi' \\ + b_8\eta f'\Phi' + b_9 f^2\Phi'' + b_{10} ff'\Phi' + b_{11} f\theta''' \\ + b_{12}\eta^2\Phi'' + b_{13}\eta\theta'' \end{bmatrix} = 0, \tag{43}$$

$$N_f = R_e\left(ff''' + \beta\left(f' - \frac{1}{2}\eta f''\right)\right) - f'f'' - \left(M^2 + \frac{1}{D_a}\right) f'' + G_r\theta' + G_c\Phi', \tag{44}$$

$$N_\theta = a_3\theta'' + a_4 f\theta' + a_5\theta'\Phi' + a_6\theta'^2 + a_7\eta^2\theta'' + a_8\eta\theta' + a_9\eta f'\theta' + a_{10}\eta f\theta'' + a_{11} f^2\theta'' + a_{12} ff'\theta' + a_{13}\eta\theta'\Phi'' + a_{14}\eta\theta''\Phi' + a_{15} f\theta'\Phi'' + a_{16} f\theta''\Phi' + a_{17}\eta\theta'\theta'' + a_{18} f\theta\theta' + a_{19}\theta + a_{20}\eta\theta' + a_{21} f\theta' + a_{22}\theta'. \tag{45}$$

where, N_f and N_θ are the nonlinear parts of f and θ respectively.

To obtain the initial guesses for the stream function f, temperature θ, and nanoparticles concentration Φ distributions, we can introduce the linear operators as follows:

$$\mathrm{L}_1(\mathrm{F}) = \mathrm{R}_e(1+\varepsilon)\frac{d^4 f}{\mathrm{d}\eta^4}, \tag{46}$$

$$\mathrm{L}_2(\theta) = \frac{d^3\theta}{\mathrm{d}\eta^3}, \tag{47}$$

$$\mathrm{L}_3(\Phi) = b_1\frac{d^2\Phi}{\mathrm{d}\eta^2}. \tag{48}$$

Where, L_1 represents the linear operator for f. Meanwhile, L_2 exinites the linear operator for θ and L_3 introduced the linear operator for Φ. Thus, the initial guesses solutions can be assumed as follows:

$$f_0 = c_1\eta^3 + c_2\eta^2 + c_3\eta + c_4, \tag{49}$$

$$\theta_0 = c_5\eta^2 + c_6\eta + c_7, \tag{50}$$

$$\Phi_0 = c_8\eta + c_9. \tag{51}$$

By substituting from Eq. (40) into the foregoing system of Eqs. (41) – (45) and collecting the terms of like powers of P on all of them, zero-order, first order, and second-order systems of nonlinear ordinary differential equations can be obtained. Finally, solve the resulted linear system of equations. One obtains the semi-analytic solutions of the various stages of P^n. The process is lengthy, but straightforward. The entire solution is gained by setting $P=1$. The solutions are calculated up to second order. Thus, all complete solutions for the

previous three distributions may be written as follows:

$$f(\eta)=A_1\eta^{14}+A_2\eta^{13}+A_3\eta^{12}+A_4\eta^{11}+A_5\eta^{10}+A_6\eta^9+A_7\eta^8+A_8\eta^7+A_9\eta^6+A_{10}\eta^5+A_{11}\eta^4+\frac{1}{6}(S_1+S_{10}+S_{19})\eta^3+\frac{1}{2}(S_2+S_{11}+S_{20})\eta^2+(S_3+S_{12}+S_{21})\eta+(S_4+S_{13}+S_{22}), \quad (52)$$

$$f'(\eta)=14A_1\eta^{13}+13A_2\eta^{12}+12A_3\eta^{11}+11A_4\eta^{10}+10A_5\eta^9+9A_6\eta^8+8A_7\eta^7+7A_8\eta^6+6A_9\eta^5+5A_{10}\eta^4+4A_{11}\eta^3+\frac{1}{2}(S_1+S_{10}+S_{19})\eta^2+(S_2+S_{11}+S_{20})\eta+(S_3+S_{12}+S_{21}), \quad (53)$$

$$\theta(\eta)=A_{12}\eta^{22}+A_{13}\eta^{21}+A_{14}\eta^{20}+A_{15}\eta^{19}+A_{16}\eta^{18}+A_{17}\eta^{17}+A_{18}\eta^{16}+A_{19}\eta^{15}+A_{20}\eta^{14}+A_{21}\eta^{13}+A_{22}\eta^{12}+A_{23}\eta^{11}+A_{24}\eta^{10}+A_{25}\eta^9+A_{26}\eta^8+A_{27}\eta^7+A_{28}\eta^6+A_{29}\eta^5+A_{30}\eta^4+A_{31}\eta^3+\frac{1}{2}(S_5+S_{14}+S_{23})\eta^2+(S_6+S_{15}+S_{24})\eta+(S_7+S_{16}+S_{25}), \quad (54)$$

$$\Phi(\eta)=A_{32}\eta^{14}+A_{33}\eta^{13}+A_{34}\eta^{12}+A_{35}\eta^{11}+A_{36}\eta^{10}+A_{37}\eta^9+A_{38}\eta^8+A_{39}\eta^7+A_{40}\eta^6+A_{41}\eta^5+A_{42}\eta^4+A_{43}\eta^3+A_{44}\eta^2+(S_8+S_{17}+S_{26})\eta+(S_9+S_{18}+S_{27}). \quad (55)$$

Where, the arbitrary constants (S_1-S_{27}) and the coefficients (A_1-A_{44}) that appeared in Eqs. (52) - (55), are not included in the manuscript to save the length. They are available under the request of the referees.

4.2. Convergence of homotopy perturbation method:

Suppose that the solution of equations (25) - (27) can be written as a power series as follows

$$n(r,P)=n_0+P\,n_1+P^2\,n_2+\ldots\ldots, \quad (56)$$

where, n is one of the physical quantities f, θ, and Φ. Setting $P=1$ we obtain the semi-analytical solution of equations (25) - (27) as follows:

$$n=\lim_{p\to 1}\left(n^0+P\,n^1+P^2\,n^2+\ldots\ldots\right). \quad (57)$$

The series of equations (25) - (27) is convergent for most of all cases.

5. Results and numerical discussions

5.1. Some special cases of our current investigation:

To reduce the mathematical manipulation in resolve the resulted Eqs. (25) - (27), as some special cases of our analysis comparing with previous published studies to validate our present study.

- In case when the parameters ($R_d=0,\ \beta_1=0,\ S_r=0,$ and $R_c=0$) are excluded from our analysis. Thus, the resulted heat and nano concentration equations are in decent close to those observed in the study represented by [1].
- The consideration of the Newtonian case, and in absence the impacts of nanofluid phenomena as well as nano concentration equation. In addition, neglecting the influences of ($G_r=0,\ G_c=0,$ and $\beta=0$). One obtains the same system of equation that represented in the study of [2].
- In case when we excluded the impacts of the parameters as: ($R_d=0,\ \beta_1=0,\ S_r=0,$ and $R_c=0$). One gain the same temperature and nano concentration equations as those obtained in the previous study of [3].
- The special case when neglecting the influences of the physical parameters ($\gamma_N=0,\ R_d=0,\ \beta_1=0,\ S_r=0,$ and $R_c=0$). Both resulted temperature and nano concentration equations are in nice agreement with those observed in the study of [5].
- In the absence of porous medium effect. In addition, when the physical parameters ($G_r=0,\ G_c=0,\ \beta=0,\ R_d=0,\ \beta_1=0,\ S_r=0,$ and $R_c=0$) are disregarded from our system of equations. Hence, The resulted governing system of equations is in great consistent with the system presented in the analysis of [6].

- In case when the physical parameters ($S_r = 0,$ and $\beta_1 = 0$) are neglected. One finds both temperature and nano concentration equations that observed in the work of Atlas et al. [9].
- In the absence of nanofluid and Cattaneo-Christov heat and mass fluxes. Also, when $S_r = 0$, our resulted temperature and concentration equations are similar to that pointed out in the work presented by Ghadikolaei et al. [10].
- In the Newtonian case as well as in the absence of Cattaneo-Christov heat and mass fluxes as well as porous medium. Also, ignoring the influences of the parameters ($\beta_1 = 0, S_r = 0, G_r = 0, G_c = 0,$ and $R_d = 0$). Thus, we can find the same system of equations that reported by the published work of Hosseinzadeh et al. [11].
- The Newtonian case in the absence of Cattaneo-Christov heat and mass fluxes, porous medium and nanofluid phenomena. In addition, ignoring the impacts of the physical parameters ($G_r = 0,$ and $G_c = 0$). Consequently, our resulted governing system of equations are in great consistent with those pointed out in the published work of Thumma and Magagula [12].
- The case when the following parameters ($\gamma_E = 0, \gamma_N = 0, R_d = 0, \beta_1 = 0, S_r = 0,$ and $R_c = 0$) are neglected in our study. Hence the resulted temperature and nano concentration equations are fully complying with those elaborated in the work of Rasool et al. [13].
- The case when we ignore the effects of the parameters ($S_r = 0,$ and $R_c = 0$), one can obtain the nanoparticles concentration equation which reported by previous published works of [[24], [25], and [26]].
- In the absence of Cattaneo- Christov heat and mass fluxes. In addition, when ($S_r = 0,$ and $R_c = 0$) are excluded from our system of equation. Thus, The obtained nano concentration equation is in decent complying with this represented in the work of El Dabe et al. [33].
- In the absence of nanofluid phenomena as well as Cattaneo- Christov heat and mass fluxes. The obtained concentration equation is in great congruent with this displayed in the work of El Dabe et al. [36].
- For $\beta_1 = 0$, in addition in the absence of nanofluid as well nano concentration equation. Hence, the resulted energy equation is in good consistent with the finding of [41].
- When the parameters ($\gamma_N = 0, S_r = 0,$ and $R_d = 0$) are ignored from our study. Consequently, the resulted heat and nano concentration equations are in nice agreement with those pointed out in the work of [42].
- The Newtonian case when the physical parameters as: ($G_r = 0, G_c = 0, M = 0,$ $R_d = 0, \beta_1 = 0, S_r = 0,$ and $R_c = 0$) are excluded from our study. Then, The resulted governing equations of motion are in nice consistent with those explained in the analysis of [43].

5.2. Graphical explanation:

The essential aim of this portion is to explain the graphical demonstration for distinct quantiles of the various physical parameters on the resultant distributions. Mathematica software is employed for illustrating the quantitative impacts of the several physical parameters comprised in this study on the distributions of the velocity $f'(\eta)$, stream function $f(\eta)$, temperature θ and nanoparticles concentration Φ. The impacts of the physical parameters such as, squeezing parameter β, Eyring - Powell fluid parameter ε, magnetic field parameter M, thermal relaxation time γ_E, mass relaxation time γ_N, Reynold's number R_e, thermophoresis parameter N_t, Darcy number D_a, heat transfer Biot number B_{iT}, mass transfer Biot number B_{iC}, Brownian motion parameter N_b, Prandtl number P_r, heat generation absorption parameter β_1, Soret number S_r, chemical reaction parameter R_c, and Lewis number L_e on the above distributions are studied numerically, graphically and displayed throughout some Figs. 2-12. The ranges of the forgoing physical parameters are in decent close to those represented in the published studies of [[4], [9], [10], [11], [13], [24], [25], [26], [28], [33], [35], [43], and [45]]. These ranges can be listed as: $(P_r = 1.0,$ $M = 0.5,\ N_t = 0.5,\ N_b = 1.5,\ \gamma_E = 0.5,$

$\gamma_N = 0.5,\ L_e = 1,\ S_r = 0.5,\ R_e = 1.0,$
$B_{iC} = 0.5,$ and $\beta_1 = 1.0).$

5.2.1. velocity profiles:

The variation of the velocity $f'(\eta)$ versus η corresponding to several quantiles of the physical parameters M, D_a, and β is illustrated through Figs. (2-4). Fig.2. is sketched to scrutinize the influence of the magnetic field parameter M. In this figure it is realized that the velocity $f'(\eta)$ has a dual behaviour in terms of change of M. Thus, the value of the velocity $f'(\eta)$ decays with the improve in the values of magnetic field parameter M along the range $(0 < \eta < 0.5)$. Physiologically, magnetic field parameter elucidates the ratio between the magnetic force and the viscous force. Moreover, the application of the transverse magnetic field has an inclination to create a drag force known as Lorentz force that resists the motion of the fluid, this is in great congruent with the nature theory which states that the elevation in the value of the magnetic field parameter M leading to an improvement in the Lorentz force. It is realized that Lorentz force contrast with the flow. This displays that the flow will overburden if we elevate the strength of the magnetic field. Therefore, the fluid velocity declines. This result has an efficient role in several distinct types of industrial applications, especially in partiality to solidification processes like casting and semiconductor single crystal growth applications. In these claims, as the liquids experience solidification, fluid flow and turbulence occur in the solidifying liquid pool and have critical conclusions on the product quality control. The practice of magnetic fields has effectively been applied to monitoring melt convection in solidification systems. This behaviour is in great conformity with the represented behaviours in published by [[2], [3], [6], [10], [13], [24], [25], [41], and [44]]. On the contrary, along the range $(0.5 < \eta < 1)$ the inverse behaviour is occurred. This resulted observation is in great consistent with this explained by [44]. Fig.3. exemplify the features of the Darcy number D_a on the velocity $f'(\eta)$. It is viewed from this figure that the Darcy number D_a has a reverse impact when compared with the magnetic parameter M. Physically, Darcy number known as the capacity of the porosity of the medium. For large values of the porosity of the medium fluid acquires more space to flow as a consequence its velocity increases. This observed performance is in nice congruent to the behaviours demonstrated in the work of [[13], [14], and [44]]. Fig. 4. demonstrates the impact of the squeezing parameter β on the velocity $f'(\eta)$. It's depicting from this figure that the value of the velocity $f'(\eta)$ substantial enhancement with an elevation in the value of the squeezing parameter β. In the physical point of view, it is known that for positive values of the squeezing parameter $(\beta > 0)$, the plates moving apart. Whereas for negative values of the squeezing parameter $(\beta < 0)$, the plates move together towards each other. Hence, larger values of the squeezing parameter $(\beta > 0)$ lead to substantial boost velocities. It is due to the fact that right plate moves a part the left plate which results a force in the fluid which contribute more fluid's deformation. Therefore, the velocity profile enhances. This resultant behaviour is similar to the observed trend clarified by the published studies of [[2], [7], [9], [10], and [45]].

Also, the influences of the embedded parameters $\varepsilon, G_r, G_c,$ and $R_e.$ on the velocity $f'(\eta)$. are studied. it's recognized that they have the similar behaviour when compared with the Darcy number D_a. To avert repetition, the graphs of these parameters are disregarded here. From the physical explanation, improving in the value of Eyring - Powell parameter $(\varepsilon > 0)$ leads to a development in the fluid. in addition, the fluid flow becomes less viscous and hence the fluid velocity is substantial enriched. This observed behaviour is similar to those recognized by [[4], [5], [6], and [10]]. Furthermore, the velocity has a dual performance under the influence of both of heat and mass transfer Grashof numbers G_r and G_c, which play a significant rule in this investigation. Physically, the heat transfer Grashof number enlarge the strength of the flow. Here positive values of the thermal Grashof number $(G_r > 0)$ corresponding to the cooling problem. Moreover, cooling problem has a substantial importance and encountered in the applications of engineering, such as in the nuclear reactors and cooling of electronic components. In addition, in the presence of natural convection heat transfer, the thermal Grashof number G_r elucidates the relative influence between the natural convection buoyancy force due to spatial variation in fluid's density (caused by temperature differences ΔT) to the viscous hydrodynamic force acting on the fluid layers. It is, also, controls the ratio of length scale to natural convection thickness. As predicted, it is

detected that there is an improvement in the value of the velocity $f'(\eta)$ due to the increment of thermal buoyancy force. Also, as G_r enhances, the peak values of the velocity w boosts quickly and then decompose smoothly to the free stream velocity. Also, the mass Grashof number represents the ratio of the buoyancy force to the viscous hydrodynamic force. According to the preceding definition, the fluid velocity enriches in accordance with the enlargement in the species buoyancy force. Therefore, one can detected that the velocity magnifies with enlarging values of mass Grashof number. These detected performances are fully consistent with those pointed out in [46]. Finally, the Reynolds number exhibits the ratio between the inertial forces and the viscous forces in the fluid. Consequently, as the Reynolds number enlarges, the viscous force diminishes. In particular, low Reynold's number flows, being dominated by viscous effects, are typically laminar with little dynamic action, and are therefore more sluggish. At larger values of the Reynold's number, the flow is typically turbulent with lots of large- and small-scale swirling motions (called eddies or vortices) and the flow can be quite chaotic on small scale even when the gross flow is fairly steady and smooth on average. It is also possible to have large scale unsteadiness at high Reynold's number. This noticed conduct is fully compatible with this displayed by [44]. To save spaces and avert reptation, we disregard these figures.

5.2.2. Stream function profiles:

The variation of the stream function $f(\eta)$ versus η for distinct values of the diverse physical parameters β, M, D_a, ε, R_e, G_r and G_c is examined. Fig.5. portrays the influence of the magnetic field parameter M on the stream function $f(\eta)$. In this figure it is detected that the value of the stream function $f(\eta)$ declines with the elevation in the value of the magnetic field parameter M. Physically, the magnetic field parameter M exhibits the ratio between the magnetic force and the viscous force. In accordance with this definition, the development in the value of the magnetic field parameter M leading to an enlargement in Lorentz force, which impeded the movement of the fluid flow. Thus, a detraction behaviour is witnessed in both velocity and stream function. This decelerated performance is corresponding to this presented by [13]. On the other hand, Fig.6. reflects the characteristics of the squeezing parameter β on the stream function $f(\eta)$. It is depicted from this figure that the squeezing parameter $\beta \succ 0$ has an inverse conduct when compared with the magnetic parameter M. This increasing performance is similar to the behaviour elaborated by [45]. Fig. 7. scrutinizes the effect of the Reynold's number R_e on the stream function $f(\eta)$. It's evident from this figure that the value of the stream function $f(\eta)$ enlarges with an improvement in the value of the Reynold's number R_e. Furthermore, the impacts of the other distinct physical parameters ε, R_e, G_r and G_c on the stream function are analysed. It's demonstrated that all these parameters behave as the same as the squeezing parameter β. These figures are eschewed here to save length.

5.2.3. Temperature profiles:

The variance of the temperature θ versus η for various quantities of the parameters γ_E, x, and P_r is discussed. Fig.8. visualize the effect of the thermal relaxation time parameter γ_E on the temperature θ. it is viewed through this figure that the temperature θ diminishes with the increment in the value of thermal relaxation time parameter γ_E. from the physiological explanation, the physical parameter γ_E incarnates the supplementary effect of heat flux relaxation time which is depicted in the non-Fourier model and is absent in the classical Fourier model. The non-Fourier Cattaneo-Christov heat flux model can be return to simple Fourier law of heat conduction by setting $(\gamma_E = 0)$. Also, the rise in the value of γ_E creates a non-conducting behaviour. Furthermore, it's captured that the particles require more time to transmit heat to its contiguous particles. That leads to reduce in the value of the temperature θ. Moreover, the temperature distribution increases only in the absence of thermal relaxation time parameter γ_E. Thus, it can be recognized that the temperature profile in the case of Fourier's law is greater than the case of Cattaneo – Christov heat flux model. This resultant behaviour is in great consistent to the behaviour examined by [[1], [3], [4], [7], [14], [24], and [25]]. Fig.9. elucidates the impact of the distance x on the temperature θ. It's depicted that the temperature θ enriches with the enhancement in

the value of x. Fig. 10 exemplify the characteristics of the Prandtl number P_r on the temperature θ. It's recognized from this figure that the value of the temperature θ decays with a development in the value of the Prandtl number P_r. Physically, the Prandtl number represents the ratio of momentum diffusivity to thermal diffusivity inside the fluid, determines ratio of fluid. It is known that the small values of the Prandtl number $(P_r \leq 1)$ represents liquid metals, that have high thermal conductivity but low viscosity. Meanwhile, large values of the Prandtl number $(P_r \geq 1)$ correspond to high-viscosity oils. Specifically, Prandtl number $P_r = 0.72, 1.0,$ and 7.0 correspond to air, electrolyte solution such as salt water and water, respectively [43]. In our investigation we have taken $(P_r = 1)$ to retrieve all the graphical results. Thus, the higher values of Prandtl number $(P_r > 0)$ are representative of polymeric non-Newtonian fluids. Larger values of the Prandtl number are associated with lower thermal diffusivity. Moreover, Prandtl number is inversely proportional to thermal conductivity. Polymers possess lower thermal conductivities and hence larger Prandtl numbers than for example liquid metals. The decrement in thermal conductivity with greater Prandtl number results in a strong decrease in fluid temperatures. This obtained conduct is in good conformity with the reported behaviours of [[1], [3], [4], [5], [6], [7], [9], [13], [25], [27], and [45]].

In addition, the features of the various physical parameters R_d, B_{iT}, and β on the temperature θ are studied. It's noticed that all of them behave similar to the behaviour of the Prandtl number P_r. Physically, the decrement in fluid temperature due to the increment in the value of the radiation parameter R_d Since, according to the relation $R_d = \dfrac{16\delta_e T_h^3}{3K\beta_e}$, increasing in the thermal radiation parameter declines the mean absorption coefficient (K), hence the value of temperature decay. This obtained behaviour is similar to those presented by [[10], [12], and [44]]. The dual performance of the temperature function under the impact of the values of heat generation parameter (β_1) is studied. It can be detected that the obtained results can be divided into two categories. Along the interval $\eta \in [0, 0.8]$, there is a detraction behaviour of temperature with an improvement in the value of heat generation parameter β_1. On the contrast, along the interval $\eta \in [0.8, 1]$, there is an increment behaviour of temperature with an enhancement in the heat generation parameter β_1 is due to enlarge in exothermic chemical reaction. This resultant observation is in great conformity with those elaborated by [[10], [12], [14], and [28]]. The heat transfer Biot number is known as the measure of the interaction between conduction in the solid and convection at its surface. In the physical view, this feature is due to the fact that an enhance in the heat transfer Biot number B_{iT} leads to decay the thermal conductivity of fluid flow. Therefore, the fluid temperature is declined. This obtained trend is in great congruent with those reported by [[12], [33], and [35]]. Finally, the impact of the squeezing parameter β on the fluid temperature is discussed. It is detected that the temperature decays with an increment in the value of the squeezing parameter β. This decrement trend is caused because higher squeezing parameter β declines the squeezing force on the fluid which consequently decrements the fluid temperature. This obtained performance is holds good with those exhibits in the works of [[7], and [11]]. To save spaces these figures are averted here.

5.2.4. Nanoparticles concertation profiles:

The variance of the nanoparticles concentration Φ versus η for distinct quantities of γ_N, and N_t is analysed. Fig.11. reveals the influence of the mass relaxation time γ_N on Φ. As evident from this figure, the value of Φ enhances with an improvement in the value of the mass relaxation time γ_N. This corresponding behaviour is in good agreement with the behaviour depicted by [24]. Fig. 12 clarifies the influence of the thermophoresis parameter N_t on Φ. It is noticed that the value of nanoparticles concentration enlarges with the increment in the value of the thermophoresis parameter N_t. From the physical illustration, the thermophoresis parameter N_t that measures the influence of the thermophoretic force on the nanofluid temperature and nanoparticles concentration, Thermophoretic force known as` the force in which a nanoparticle applies physical force on another nanoparticles to move it away from the surface when the preceding gets heated due to the temperature of the sheet. An enhancement in the values of the thermophoresis parameter N_t enlarges the thermophoretic force which tends to move the

nanoparticles from a region having higher temperature to a region that has lower temperature and correspondingly an improvement in the values of nanofluid temperature and nanoparticles concentration is occurred. This performance is in good complying with those explained by [[1], [3], [6], [11], [13], [24], [25], [33], and [43]].

Moreover, the physical effects of the various distinct parameters N_b, β, and R_c on the nanoparticles concentration Φ are examined. It's viewed that N_b, β, and R_c behave similar to the performance of the mass relaxation time γ_N. from the physical explanation, Brownian motion means the random motion of particles suspended in a fluid resulting from their collision with the quick atoms or molecules in the fluid. A physical illustration of Brownian motion was presented by Einstein, who explained Brownian motion as the cumulative impact of innumerable collisions of the suspended particle with the molecules of the fluid. The nanoparticles concentration field is decrement function of Brownian parameter N_b : In fact, when the Brownian parameter N_b enhances, the collisions between fluid particles enriches and ensure lower mass transport phenomenon from heated sheet toward the cold fluid. Therefore, nanoparticles concentration field shows detraction performance. This observed performance is in agreement with those detected in the works of [[1], [3], [5], [6], [11], [13], [25], [33], and [43]]. The impact of the squeezing parameter $(\beta > 0)$ on the nanofluid concentration Φ is illustrated. The detected declination in the behaviour of the nanofluid concentration caused since the fluid is dense outside the flow channel, so when plates move apart and spaced, enhance in β leads to decrement performance of the nanofluid concentration, this observation is fully conformity with this explained by [[7], and [11]]. the influence of chemical reaction parameter R_c on the nanoparticles concentration Φ is examined. It is realized that with improving the distractive chemical reaction $(R_c > 0)$ nanofluid concentration is decayed. Physically, the positive values of the chemical reaction $(R_c > 0)$ represents the destructive chemical reaction. Meanwhile, the negative one $(R_c < 0)$ introduces the generative chemical reaction. Therefore, this diminishes performance of the nanofluid concentration is due to, chemical reaction takes place and progressively destroys the original species diffusing in the polymeric viscoelastic fluid. This, in turn, suppresses molecular diffusion of the remaining species which leads to a decline in the values of nanofluid concentration. Generally, it can be predicted that increment the chemical reaction parameter, cause decrement in the nanofluid concentration and reducing it will also enhance the nanofluid concentration. This resultant behaviour is in decent close to the behaviour realized by [10].

Also, the impacts of the embedded parameters M, G_c, and L_e. on the nanoparticles concentration Φ are examined. Again, It's recognized that M, G_c, and L_e. performed as same as the behavior of γ_N. The magnetic field parameter M is known as the ratio of magnetic force to the viscous force. Physically, more heat produces due to the resistive force (Lorentz force). Thus, temperature field enhances. Consequently, the nanofluid concentration decays. This noticed performance is fully consistent with this elaborated by [11]. The impact of mass transfer Grashof number G_c on the nanofluid concentration of the fluid has been examined by simulation. In fact, the mass transfer Grashof number $(G_c > 0)$ and the nanofluid concentration are inversely proportional to each other i.e.as G_c enriches the velocity of the fluid enlarges and hence the nanofluid concentration decays. In addition, the Lewis number L_e is recognized as a dimensionless number which exhibits the ratio of thermal diffusivity to the mass diffusivity (or) "Schmidt number to Prandtl number". Thus, the rise in the value of Lewis number L_e leads to decline the mass diffusion since the Lewis number L_e is inversely proportional to mass diffusivity. Consequently, a rise in the inter – molecular force is occurred and hence leads to decay in nanoparticles concentration. Moreover, the increment in the magnitude of the Lewis number lead to the smaller Brownian coefficient diffusion. Thus, the concentration curves are decreased as a consequence of more effective momentum transfer through molecules. This observed conduct is in nice complying with the performances represented in the works of [[1], [3], [5], [6], [7], [10], [11], [12], [13], [24], [25], [26], [27], [28], [34] and [36]].

Moreover, the influences of both mass transfer Biot number B_{ic} and Soret number S_r on the nanofluid concentration Φ are studied. On the contrast, it is found that the parameters of B_{ic} and

S_r behave as the same as the thermophoresis parameter N_t .Mass transfer Biot number exhibits the ratio of diffusive to reactive or conv mass transfer resistance, also, determines uniformity of nano concentration in solid. The nanoparticles concentration profile is detected to enrich for the increment in the values of the mass transfer Biot number B_{iN}. Physically, the larger values of the mass transfer Biot number B_{iN} recommend a deeper penetration of nanoparticles concentration. This noticed influence is in great congruent with the behaviour reported by [9]. The Soret number S_r classifies the impact of the temperature gradients inducing significant mass diffusion effects. It is detected that an enhance in the Soret number S_r leads to an enlargement in the nanofluid concentration. This noticed conduct is similar to this pointed out in the published work by [1]. All of these figures are disregarded here to save length and avert reputation.

5.3. The physical quantities of our interest:

5.3.1. the skin friction coefficient $\sqrt{R_e}C_F$:

Fig. 13 visualize the effect of the Eyring – Powell fluid parameter $\mathcal{E}$ on the skin friction coefficient $\sqrt{R_e}C_F$ with the squeezing parameter β. It is clarified from this figure, that the skin friction coefficient $\sqrt{R_e}C_F$ has a dual behaviour under the impact of the squeezing parameter β. Hence, it elevates with an enhancement in the value of the Eyring – Powell fluid parameter $\mathcal{E}$ via the interval $\beta \in [0, 0.6]$. Meanwhile, along the interval $\beta \in [0.65, 1]$ the inverse conduct occurred. This obtained performance is in decent close to the behaviour elaborated by the work of [5]. Fig. 14 reveals the influence of the magnetic field parameter M on the skin friction coefficient $\sqrt{R_e}C_F$ with the squeezing parameter β. It is detected from this figure, that the skin friction coefficient $\sqrt{R_e}C_F$ decays with an elevation in the value of the magnetic parameter M.

5.3.2. the nano Sherwood number Sh_x :

Finally, the impact of the Brownian motion parameter N_b on the nano Sherwood number Sh_x versus the thermophoresis parameter N_t is depicts throughout Fig. 15. As viewed from this figure, the nano Sherwood number Sh_x has a dual performance under the influence of N_b. Therefore, it enhances with an improvement in the value of Brownian motion parameter N_b along the interval $N_t \in [0, 0.5]$. However, at the interval $N_t \in [0.5, 1]$ the vis versa occurred. Also, Nano Sherwood number Sh_x that, also, known as "the mass transfer Nusselt number", introduces the ratio between the rate of convective mass transport of the nanoparticles (which is due to their flow within the fluid) and the rate of diffusive mass transport of them (that caused by their random motion). Sh_x is used to compute mass transfer coefficient.

Fig(2)

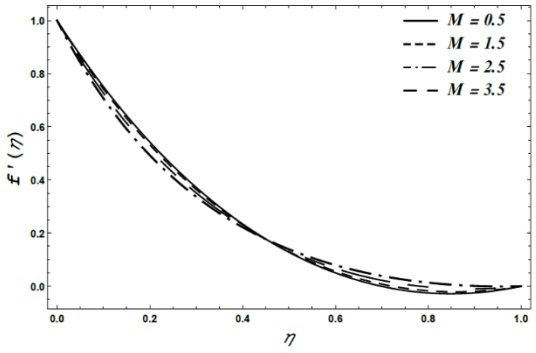

Fig(3)

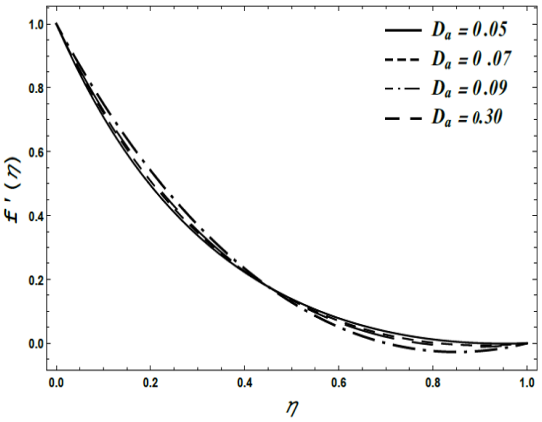

Fig(4)

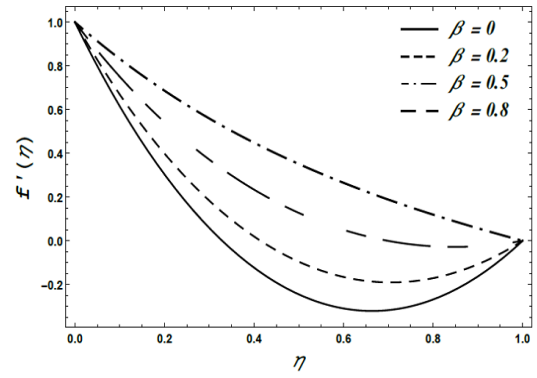

Fig(5)

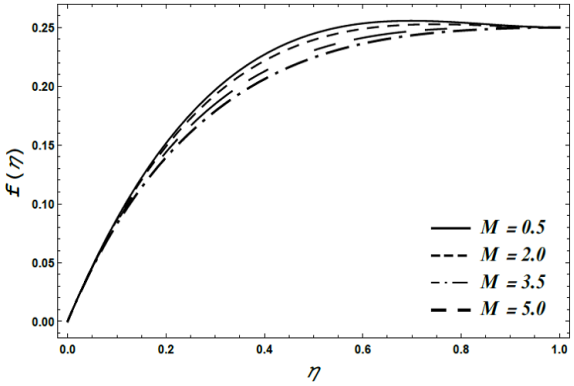

Fig(6)

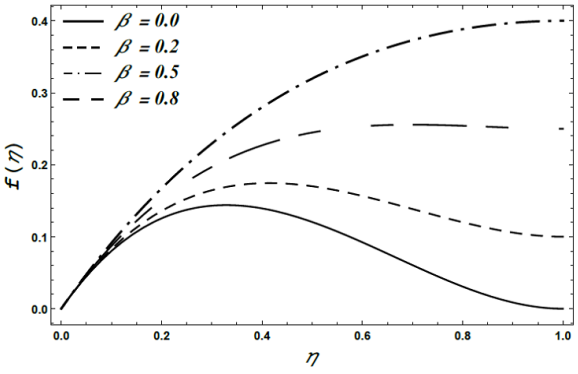

Fig(7)

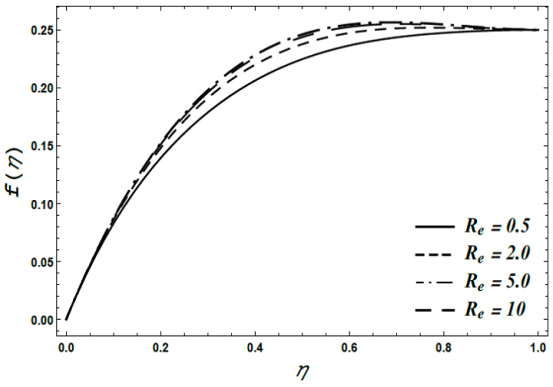

Fig(8)

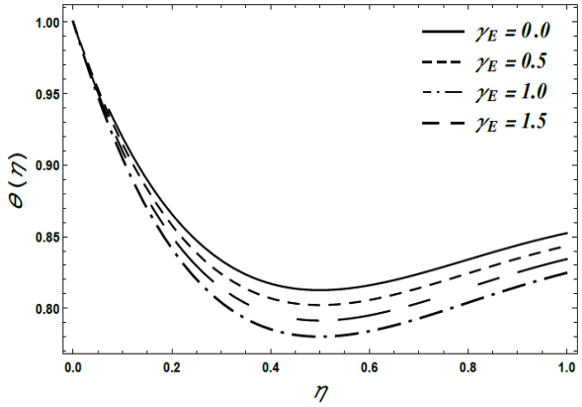

Fig(9)

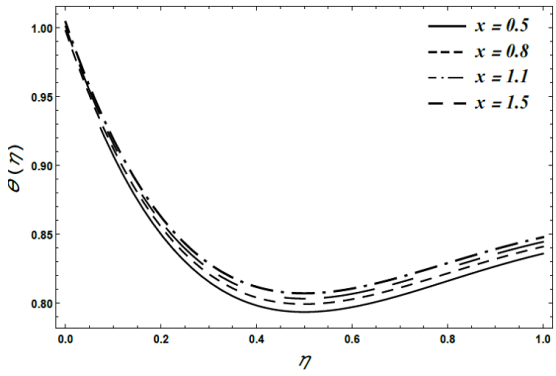

Fig(10)

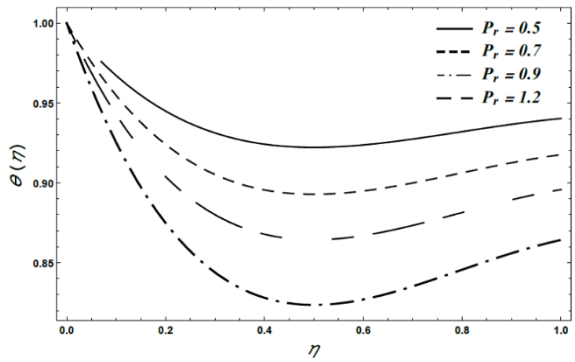

Fig(11)

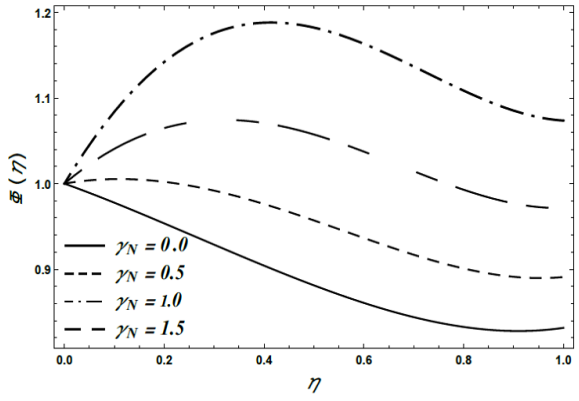

Fig(12)

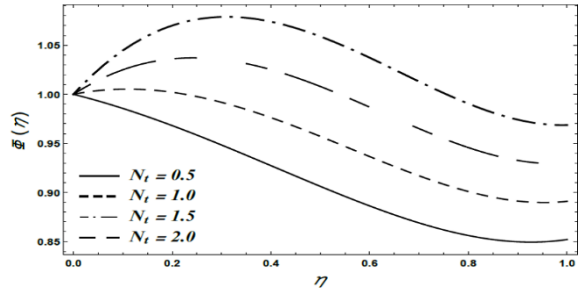

Fig(13)

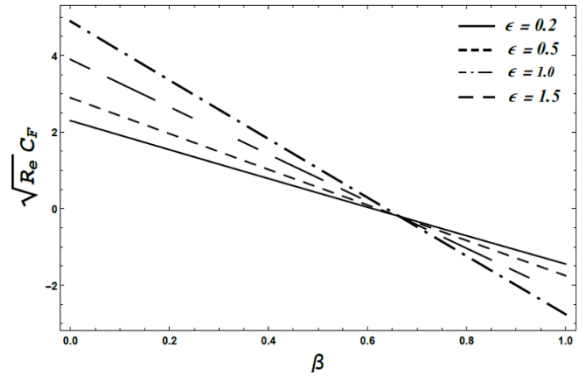

Fig(14)

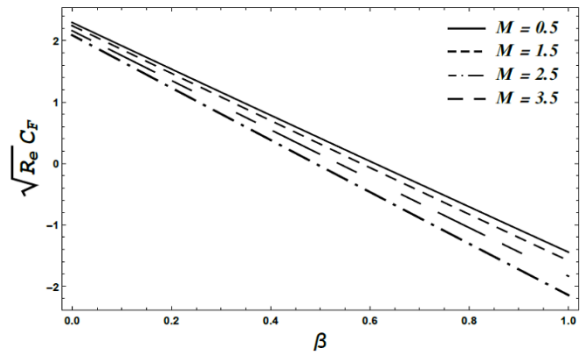

Fig(15)

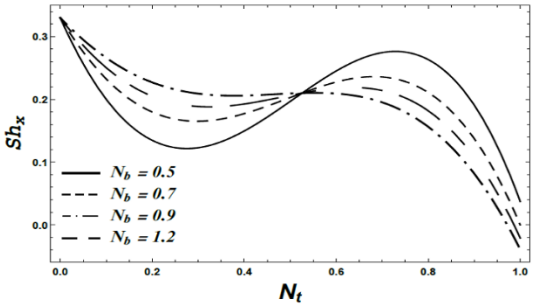

6. Conclusion

The principal objective in this study is to focus on the influence of Cattaneo-Christov double diffusion (CCDD) model on squeezing Eyring - Powell nanofluid between two parallel vertical plates in the presence of time. In addition, porous medium, thermal radiation, heat generation as well as uniform magnetic field are taken into account. Variable surface temperature and convected boundary conditions for both temperature and nanofluid concentration are also considered. A proper similarity transformation is utilized to convert our system from non-linear partial differential equations to ordinary differential equations for make it easy to solve. Homotopy perturbation method (up to the second order) is utilized to obtain the semi-analytical solution for the velocity, stream function, temperature, and nanoparticles concentration distributions. The effects of the different physical embedded parameters on these distributions are discussed numerically as well as graphically and represented via a set of draws. Finally, the distinct physical quantities of the skin friction coefficient and nano Sherwood number are computed and presented graphically throughout some graphs. The main outcomes of the present investigation are summarized as follows:

1- The magnetic field parameter M has an inverse conduct when compared with Darcy number D_a on the velocity $f(\eta)$.

2- The increment in the value of the squeezing parameter β leads to an improve in both values of the velocity and stream function. Whilst the temperature $\theta(\eta)$ and nanofluid concentration $\Phi(\eta)$ decline with an enhancement the value of β.

3- The thermal relaxation time γ_E leads to a decrement in the value of the temperature $\theta(\eta)$.

4- The enlarge in the value of the mass relaxation time γ_N enhances the value of the nanoparticles concentration $\Phi(\eta)$.

5- Nano Sherwood number Sh_x has a dual performance with the thermophoresis parameter under the influence of the Brownian motion parameter N_b.

6- The Newtonian case of this investigation can be represented by setting $(\varepsilon = 0)$.

The foregoing results may have applied substantial importance in various fields concerned in studying the squeezing non-Newtonian nanofluid in the presence of time. through two parallel vertical plates, under the impact of Cattaneo-Christov double diffusion. Moreover, from the physical demonstration, this investigation of squeezing flow has great attention in view of several applications. Such as food, compression and injection shaping, polymer industries and liquid-metal lubrication, etc. the obtained results from our research can be utilized in the following applications: chemical injection systems, develops and manufactures wellhead control panels, and Including wellhead safety control systems, metallurgical process, polymer. Furthermore, this study is related in squeezing film pressure sensors, flow rheostats, bearings, and food processing [47-72].

Nomenclature

B_{iC}	Biot number for nano concentration
B_{iT}	Biot number for heat transfer
b	Expansion / contraction strength coefficient parameter
B_0	Magnetic field strength
C	Dimensional Fluid concentration
C_f	Convective nanoparticles of the right wall
C_h	Ambient nanoparticles of the left wall
c_f	Specific heat parameter of nanoparticle
c_p	Specific heat parameter of nanoparticle
D_a	Darcy number
D_B	Brownian diffusion coefficient
D_T	Thermophoretic diffusion
$f(\eta)$	Dimensionless stream function
$\underline{g}$	Acceleration gravity
G_r	Thermal Grashof number
G_c	Nanoparticles Grashof number
$\frac{j^*}{K}$	Cattaneo Christov mass flux Thermal conductivity
K_p	Permeability of porous medium
K_T	Thermal diffusion ratio
K_1	Chemical reaction rate
L_e	Lewis number
M	Magnetic field parameter
N_b	Brownian motion parameter
N_t	Thermophoresis parameter
p	Fluid pressure
p_r	Prandtl number
$\underline{q}$	Cattaneo heat flux vector
q_m	Heat flux from surface
q_w	Nano concentration flux
R_c	Chemical reaction parameter
R_d	Radiation parameter
R_e	Reynold's number
S_r	Soret number
t	Time
T	Fluid temperature
T_f	Convective fluid temperature of the right plate
T_h	Ambient Temperature of the left plate
T_m	Mean fluid temperature

Greek symbols

α	Non dimensional parameter
α_T	Thermal expansion coefficient
α_C	Nano expansion coefficient
β	squeezing parameter
β_e	Absorption constant
c, β_r	Fluid parameters
δ_E	Thermal relaxation time
δ_N	Nano relaxation time

δ_e	Stefan-Boltzmann constant
ε	Eyring – Powell fluid parameter
γ_E	Relaxation time of mass transfer
γ_N	Relaxation time of heat transfer
η	Dimensionless variable
μ_f	Fluid viscosity
ν_f	Kinematic viscosity
θ	Dimensionless temperature
Φ	Dimensionless nanoparticle phenomena
ρ_f	Fluid density
ρ_p	Nanoparticle density
$(\rho c)_f$	Heat capacity of the fluid
$(\rho c)_p$	Effective heat capacity of fluid Material
σ	Electrical conductivity
τ	Ratio between effective heat & fluid capacity
τ_w	Shear stress

.

References

[1] M. Ramzan, A. Liaquet, S. Kadry, S. Yu, Y. Nam and D. Lu, Impact of second-order slip and double stratification coatings on 3D MHD Williamson nanofluid flow with Cattaneo–Christov heat flux, *Coatings*, **9** (2019), 1 - 20.

[2] A.S. Dogonchi and D.D. Ganji, Impact of Cattaneo–Christov heat flux on MHD nanofluid flow and heat transfer between parallel plates considering thermal radiation effect, *Journal of the Taiwan Institute of Chemical Engineers*, (2017), 1 - 12.

[3] S. A. Shehzad, S. U. Khan, Z. Abbas and A. Rauf, A revised Cattaneo-Christov micropolar viscoelastic nanofluid model with combined porosity and magnetic effects, *Applied Mathematics and Mechanics (English Edition)*, **41** (3) (2020), 521 - 532.

[4] T. Hayat and M. I. Khan, Waqas M., Alsaedi A., On Cattaneo–Christov heat flux in the flow of variable thermal conductivity Eyring–Powell fluid, *Results in Physics*, **7** (2017)., 446 - 450.

[5] W. Ibrahim, Three-dimensional rotating flow of Powell-Eyring nanofluid with non-Fourier's heat flux and non-Fick's mass flux theory, *Results in Physics*, **8** (2018), 569 – 577.

[6] W. Ibrahim and B. Hindebu, Magnetohydrodynamic (MHD) boundary layer flow of Eyring-Powell nanofluid past stretching cylinder with Cattaneo-Christov heat flux model, *Nonlinear Engineering – De Gruyter*, **8** (2019), 303–317.

[7] M. Farooq, S. Ahmad, M. Javed and A. Anjum, Analysis of Cattaneo-Christov heat and mass fluxes in the squeezed flow embedded in porous medium with variable mass diffusivity, *Results in Physics*, **7** (2017), 3788 - 3796.

[8] MJ. Stefan, Versuch über die scheinbare adhesion. Sitzungsber Sächs Akad Wiss Wein, *Math-Nat Wiss Kl*, **69** (1874), 713 - 722.

[9] M. Atlas, S. Hussain and M. Sagheer, Entropy generation and unsteady Casson fluid flow squeezing between two parallel plates subject to Cattaneo-Christov heat and mass flux, *Eur. Phys. J. Plus*, **134** (2019), 1 - 17.

[10] S.S. Ghadikolaei, Kh. Hosseinzadeh and D.D. Ganji, Analysis of unsteady MHD Eyring-Powell squeezing flow in stretching channel with considering thermal radiation and Joule heating effect using AGM, *Case Studies in Thermal Engineering*, **10** (2017), 579 - 594.

[11] Kh. Hosseinzadeh, M. Alizadeh and D. D. Ganji, Hydrothermal analysis on MHD squeezing nanofluid flow in parallel plates by analytical method, International, *Journal of Mechanical and Materials Engineering*, (2018), 1 - 13, doi: https://doi.org/10.1186/s40712-018-0089-7 .

[12] Th. Thumma and V. M. Magagula, Transient electromagnetohydrodynamic radiative squeezing flow between two parallel Riga plates using a spectral local linearization approach, *Heat Transfer Asian Research*, (2019), 68 - 85, doi: 10.1002/htj.21599.

[13] Gh. Rasool, W. A. Khan, S. M. Bilal, and I. Khan, MHD squeezed Darcy–Forchheimer nanofluid flow between two h–distance apart horizontal plates, *Open Physics - De Gruyter*, **18** (2020), 1100 - 1107.

[14] F. Shah, M. I. Khan, T. Hayat, Sh. Momani, and M. I. Khan, Cattaneo-Christov heat flux (CC model) in mixed convective stagnation point flow towards a Riga plate, *Comput Methods Programs Biomed*, (2020), 1 - 17, doi: https://doi.org/10.1016/j.cmpb.2020.105564.

[15] N. T. M. El-dabe, M. Y. Abou-zeid and Y. M Younis. , Magnetohydrodynamic peristaltic flow of Jeffry nanofluid with heat transfer through a porous medium in a

vertical tube, *Applied Mathematics & Information Science*, **11** (4) (2017), 1097-1103.

[16] N. T. M. El-dabe, and S. N. Sallam, Non-Darcy Couette flow through a porous medium of magnetohydrodynamic viscoelastic fluid with heat and mass transfer, *Canadian Journal of Physics*, **83** (12) (2011), 1243-1265.

[17] N. T. M. El-dabe, G. Saddeek, A. F. El Sayed, Heat transfer of MHD non-Newtonian Casson fluid flow between two rotating cylinders, *Mechanics and Mechanical Engineering*, **5** (2) (2001), 237-251.

[18] N. T. M. El-dabe and M. A.A. Mohamed, Heat and mass transfer in hydromagnetic flow of the non-Newtonian fluid with heat source over an accelerating surface through a porous medium, *Chaos Solitons & Fractals*, **13** (4) (2002),:907-917.

[19] N. T. M. El-dabe, M. A. Hassan, M. Y. Abou-Zeid, Wall properties effect on the peristaltic motion of a coupled stress fluid with heat and mass transfer through a porous medium, *Journal of Engineering Mechanics*, **142** (3) (2016), (04015102-1) – (04015102-9).

[20] N. T. M. El-dabe and M. Y. Abou-zeid, Radially varying magnetic field effect on peristaltic motion with heat and mass transfer of a non-Newtonian fluid between two co-axial tubes, *Thermal Science*, **22** (6 A) (2018), 2449-2458.

[21] J.B. Fourier, Theorie analytique, De La Chaleur Paris, (1822).

[22] C. Cattaneo, Sulla conduzione del calore, Atti. Semin. Mat. Fis. Univ. *Modena Reggio Emilia*, **3** (1948), 89 - 101.

[23] C. I. Christov, On frame indifferent formulation of the Maxwell – Cattaneo model of finite – speed heat conduction, *Mech. Res. Commun*., **36** (2009), 481- 486.

[24] M. I. Khan, M. U. Hafeez, T. Hayat and A. Alsaedi, Fully developed Darcy-Forchheimer nanomaterial ow with Cattaneo Christov (CC) double diffusion model, **Modern Physics Letters B**, (2020), (2050214-1) - (2050214-16), doi:10.1142/S0217984920502140.

[25] S. Masood, M. Farooq and Sh. Ahmad, Description of viscous dissipation in magnetohydrodynamic flow of nanofluid: Applications of biomedical treatment, *Advances in Mechanical Engineering*, **12** (6) (2020), 1 - 13.

[26] T. Hayat, S. A. Khan, M. I. Khan, Sh. Momani and A. Alsaedi, Cattaneo-Christov (CC) heat flux model for nanomaterial stagnation point flow of Oldroyd-B fluid, *Computer Methods and Programs in Biomedicine*, **187** (2020), 1 -7.

[27] U. Nazir, S. Saleem, M. Nawaz, M. A. Sadiq and A.A. Alderremy, Study of transport phenomenon in Carreau fluid using Cattaneo–Christov heat flux model with temperature dependent diffusion coefficients, *Physica A*, **554** (2020), 1 - 14.

[28] Sh. Ahmad and S. Nadeem, Flow analysis by Cattaneo–Christov heat flux in the presence of Thomson and Troian slip condition, *Applied Nanoscience*, **10** (2020), 4673 – 4687.

[29] J. H. He, Homotopy perturbation technique. *Comput. Methods Appl. Mech. Eng.* **178** (3) (1999), 257 - 262.

[30] M. Y. Abou-zeid, Effects of thermal - diffusion and viscous dissipation on peristaltic flow of micropolar non-Newtonian nanofluid: Application of homotopy perturbation method, *Results Phys*. **6** (2016), 481 - 495.

[31] M. Y. Abou-zeid, Homotopy perturbation method to MHD non- Newtonian nanofluid flow through a porous medium in eccentric annuli with peristalsis, *Thermal Sci.*, (2015), 1 - 16.

[32] N. T. M. Eldabe, M. Y. Abou-zeid, and O. S. Ahmed, Motion of a thin film of a fourth grade nanofluid with heat transfer down a vertical cylinder: homotopy perturbation method application, *Journal of Advanced Research in Fluid Mechanics and Thermal Sciences*, **66** (2) (2020), 101 - 113.

[33] M. El. M. Ouaf and M. Y. Abou-zeid, Hall currents effect on squeezing flow of non-Newtonian nanofluid through a porous medium between two parallel plates, *Case Studies in Thermal Engineering*, **28** (2021), 101362.

[34] N. T. Eldabe, G. M. Moatimid and A. Sayed, Effect of the magnetic induction on the peristaltic Eyring-Prandtl nanofluid through porous medium, *International Journal of Applied Electromagnetics and Mechanics*, **63** (2020), 279 - 298

[35] N. T. Eldabe and D. R. Mostapha, Hall current effects on electro-magneto-dynamic peristaltic flow of an Eyring–Powell fluid with mild stenosis through a uniform and non-uniform annulus, *Indian Journal of Physics*, (2021), 1 - 13. doi:

https://doi.org/10.1007/s12648-021-02185-z.

[36] N. T. M. Eldabe, G. M. Moatimid, M. A. A. Mohamed, Y. M. Mohamed, Effects of Hall currents with heat and mass transfer on the peristaltic transport of a Casson fluid through a porous medium in a vertical circular cylinder, *Thermal Science*, **24** (2B) (2020), 1067 - 1081.

[37] N. T. M. El-dabe, A. Shaaban, M. Y. Abou-zeid and H. A. Ali, Magnetohydrodynamic non-Newtonian nanofluid flow over a stretching sheet through a non-Darcy porous medium with radiation and chemical reaction, *Journal of Computational and Theoretical Nanoscience*, **12** (12) (2015), 5363 -5371.

[38] M. Y. Abou-zeid, Implicit homotopy perturbation method for MHD non-Newtonian nanofluid flow with Cattaneo-Christov heat flux due to parallel rotating disks, *Journal of nanofluids*, **8** (8) (2019), 1648-1653.

[39] N. T. El-dabe, Magnetohydrodynamic unsteady free convective flow through a porous medium bounded by an infinite vertical porous plate, *Canadian Journal of Physics*, **64** (1) (1986), 84-89.

[40] J. A. Shereliff, A textbook of magnetohydrodynamics, Pergamon Press - Oxford (1965).

[41] A. Mahmood, W. Jamshed and A. Aziz, Entropy and heat transfer analysis using Cattaneo-Christov heat flux model for a boundary layer flow of Casson nanofluid, *Results in Physics*, **10** (2018), 640 - 649.

[42] H. Mondal and P. Sibanda, Spectral Quasi-Linearization Method for entropy generation using the Cattaneo–Christov heat flux model, *International Journal of Computational Methods*, **16** (3) (2019), (1940002-1) - (1940002-18).

[43] M. M. Hashmi, T. Hayat, and A. Alsaedi, On the analytic solutions for squeezing flow of nanofluid between parallel disks, *Nonlinear Analysis: Modelling and Control*, **17** (4) (2012), 418 - 430.

[44] N. T. M. Eldabe, M. Y. Abou-zeid, M. A. A. Mohamed and M. M. Abd-Elmoneim, MHD peristaltic flow of non-Newtonian power-law nanofluid through a non-Darcy porous medium inside a non-uniform inclined channel, *Archive of Applied Mechanics*, **91** (2021), 1067–1077.

[45] M. Zubair, Z. Shah, S. Islam, W. Khan and A. Dawar, Study of Three-dimensional Darcy–Forchheimer squeezing nanofluid flow with Cattaneo–Christov heat flux based on four different types of nanoparticles through entropy generation analysis, *Advances in Mechanical Engineering*, **11** (5) (2019), 1-17.

[46] K. Ramesh and M. Devakar, Effects of endoscope on the peristaltic transport of a couple stress fluid with heat transfer: *Application to biomedicine, Nonlinear Engineering*, **8** (2019), 619-629.

[47] M. El. Ouaf and M. Abou-zeid, Electromagnetic and non-Darcian effects on a micropolar non-Newtonian fluid boundary-layer flow with heat and mass transfer, *International Journal of Applied Electromagnetics and Mechanics*, **66** (2021), 693-703.

[48] N. T. Eldabe, M. Y. Abou-zeid, O. H. El-Kalaawy, S. M. Moawad and O.S Ahmed, Electromagnetic steady motion of Casson fluid with heat and mass transfer through porous medium past a shrinking surface, *Thermal Science*, **25** (1A) (2021), 257-265.

[49] N. T. M. Eldabe, M. Y. Abou-zeid, S. M. Elshabouri, T. N. Salama and A. M. Ismael, Ohmic and viscous dissipation effects on micropolar non-Newtonian nanofluid Al2O3 flow through a non-Darcy porous media, *International Journal of Applied Electromagnetics and Mechanics*, **68** (2022), 209-221.

[50] N. T. M. Eldabe, R. R. Rizkallah, M. Y. Abou-zeid and V. M. Ayad, Thermal diffusion and diffusion thermo effects of Eyring- Powell nanofluid flow with gyrotactic microorganisms through the boundary layer, *Heat Transfer - Asian Res.*, **49** (2020), 383 – 405.

[51] N. T. Eldabe, G. M. Moatimid, M. Y. Abouzeid, A. A. ElShekhipy and N. F. Abdallah, A semianalytical technique for MHD peristalsis of pseudoplastic nanofluid with temperature- dependent viscosity: Application in drug delivery system, *Heat Transfer-Asian Research*, **49** (2020), 424–440.

[52] N. T. M. Eldabe, G. M. Moatimid, M. Abou-zeid, A. A. Elshekhipy and N. F. Abdallah, Semi-analytical treatment of Hall current effect on peristaltic flow of Jeffery nanofluid, *International Journal of Applied Electromagnetics and Mechanics*, **7** (2021), 47-66.

[53] N. T. M. Eldabe, M. Y. Abou-zeid, A. Abosaliem, A. Alana, and N. Hegazy, Homotopy perturbation approach for Ohmic dissipation and mixed convection effects on non-Newtonian nanofluid flow between two co-axial tubes with peristalsis, *International Journal of Applied Electromagnetics and Mechanics*, **67** (2021), 153-163.

[54] N. T. Eldabe, M. Y. Abou-zeid, M. A. Mohamed and M. Maged, Peristaltic flow of Herschel Bulkley nanofluid through a non-Darcy porous medium with heat transfer under slip condition, *International Journal of Applied Electromagnetics and Mechanics*, **66** (2021), 649-668.

[55] N. T. M. Eldabe, G. M. Moatimid, M. Abou-zeid, A. A. Elshekhipy and N. F. Abdallah, Instantaneous thermal-diffusion and diffusion-thermo effects on Carreau nanofluid flow over a stretching porous sheet, *Journal of Advanced Research in Fluid Mechanics and Thermal Sciences,* **72** (2020) 142-157.

[56] N. T. M. Eldabe, M. Y. Abou-zeid, M. E. Ouaf, D. R. Mostapha and Y. M. Mohammed, Cattaneo – Christov heat flux effect on MHD peristaltic transport of Bingham Al_2O_3 nanofluid through a non – Darcy porous medium, *International Journal of Applied Electromagnetics and Mechanics*, **68** (2022), 59-84.

[57] M.Y. Abou-zeid, Homotopy perturbation method to gliding motion of bacteria on a layer of power-law nanoslime with heat transfer, *Journal of Computational and Theoretical Nanoscience*, **12** (2015), 12:3605-3614.

[58] M. A. Mohamed and M.Y. Abou-zeid, MHD peristaltic flow of micropolar Casson nanofluid through a porous medium between two co-axial tubes, *J. porous media*, **22** (2019), 1079–1093.

[59] M.Y. Abou-zeid, Homotopy perturbation method for couple stresses effect on MHD peristaltic flow of a non-Newtonian nanofluid, *Microsystem Technologies*, **24** (2018) 4839–4846.

[60] M. Y. Abou-zeid, Magnetohydrodynamic boundary layer heat transfer to a stretching sheet including viscous dissipation and internal heat generation in a porous medium, *Journal of porous Media*, **14** (11) (2011), 1007-1018.

[61] M. Y. Abou-zeid, A. A. Shaaban, and M. Y. Alnour, Numerical treatment and global error estimation of natural convective effects on gliding motion of bacteria on a power-law nanoslime through a non-Darcy porous medium, *Journal of Porous Media*, **18** (2015), 1091–1106.

[62] M. Y. Abou-zeid, and M. A. A. Mohamed, Homotopy perturbation method for creeping flow of non-Newtonian Power-Law nanofluid in a nonuniform inclined channel with peristalsis. *Z. Naturforsch*, **72** ((10)a) (2017), 899–907.

[63] A. Ismael, N. Eldabe, M. Abouzeid and S. Elshabouri, Activation energy and chemical reaction effects on MHD Bingham nanofluid flow through a non-Darcy porous media, *Egyptian Journal of Chemistry*, **65** (2022), 715 – 722.

[64] M. E. Ouaf, M. Y. Abouzeid and Y. M. Younis, Entropy generation and chemical reaction effects on MHD non-Newtonian nanofluid flow in a sinusoidal channel, *International Journal of Applied Electromagnetics and Mechanics*, **69** (2022), 45-65.

[65] M. Ibrahim, N. Abdallah and M. Abouzeid, Activation energy and chemical reaction effects on MHD Bingham nanofluid flow through a non-Darcy porous media, *Egyptian Journal of Chemistry*, Doi: 10.21608/EJCHEM.2022.117814.5310.

[66] N. T. Eldabe, S. Elshabouri, H. Elarabawy, M. Y. Abouzeid and A. Abuiyada, Wall properties and Joule heating effects on MHD peristaltic transport of Bingham non-Newtonian nanofluid , *International Journal of Applied Electromagnetics and Mechanics*, **69** (2022), 87 – 106.

[67] N. T. M. Eldabe, R. R. Rizkallah, M. Y. Abou-zeid and V. M. Ayad, Effect of induced magnetic field on non-Newtonian nanofluid Al2IO3 motion through boundary-layer with gyrotactic microorganisms, *Thermal Science*, **26** (2022), 411 – 422.

[68] N. T. M. Eldabe, M. Y. Abouzeid, and H.A. Ali, Effect of heat and mass transfer on Casson fluid flow between two co-axial tubes with peristalsis, *J. Adv. Res. Fluid Mech. Therm. Sci*. **76** (1) 2020 54-75.

[69] H. M. Mansour and M. Y. Abouzeid, Heat and mass transfer effect on non-newtonian fluid flow in a non-uniform vertical tube with peristalsis, J. Adv. Res. Fluid Mech. *Therm. Sci.*, **61** (1) (2019) 44-64.

[70] N. T. M. Eldabe, M. Y. Abou-zeid, A. Abosaliem, A. Alana, and N. Hegazy, Thermal Diffusion and Diffusion Thermo Effects on Magnetohydrodynamics Transport of Non-Newtonian Nanofluid Through a Porous Media Between Two Wavy Co-Axial Tubes, *IEEE Transactions on Plasma Science*, **50** (2021), 1282-1290.

[71] N.T. Eldabe, M.Y. Abou-zeid and H.A. Shawky, MHD peristaltic transport of Bingham blood fluid with heat and mass transfer through a non-uniform channel,

J. Adv. Res. Fluid Mech. Therm. Sci., **77** (2021), 145–159.

[72] M. Y. Abouzeid, A Chemical reaction and non-Darcian effects on MHD generalized Newtonian nanofluid motion, *Egyptian Journal of Chemistry*, Doi: 10.21608/EJCHEM.2022.132580.5857.